HHS Public Access

Author manuscript

Cell Rep. Author manuscript; available in PMC 2020 March 17.

Published in final edited form as:

Cell Rep. 2020 February 25; 30(8): 2481–2488.e5. doi:10.1016/j.celrep.2020.02.002.

Rocaglates Induce Gain-of-Function Alterations to eIF4A and eIF4F

Jennifer Chu[1], **Wenhan Zhang**[2,9], **Regina Cencic**[1,9], **Patrick B.F. O'Connor**[3,9], **Francis Robert**[1], **William G. Devine**[2], **Asher Selznick**[1], **Thomas Henkel**[4], **William C. Merrick**[5], **Lauren E. Brown**[2], **Pavel V. Baranov**[3,6], **John A. Porco Jr.**[2,*], **Jerry Pelletier**[1,7,8,10,*]

[1]Department of Biochemistry, McGill University, Montreal, QC, Canada [2]Department of Chemistry and Center for Molecular Discovery (BU-CMD), Boston University, Boston, MA, USA [3]School of Biochemistry and Cell Biology, University College Cork, Cork, Ireland [4]IMAX Discovery GmbH, Dortmund, Germany [5]Department of Biochemistry, School of Medicine, Case Western Reserve University, Cleveland, OH 44106-4935, USA [6]Shemyakin-Ovchinnikov Institute of Bioorganic Chemistry RAS, Moscow, Russia [7]Department of Oncology, McGill University, Montreal, QC, Canada [8]Rosalind & Morris Goodman Cancer Research Centre, McGill University, Montreal, QC, Canada [9]These authors contributed equally [10]Lead Contact

SUMMARY

Rocaglates are a diverse family of biologically active molecules that have gained tremendous interest in recent years due to their promising activities in pre-clinical cancer studies. As a result, this family of compounds has been significantly expanded through the development of efficient synthetic schemes. However, it is unknown whether all of the members of the rocaglate family act through similar mechanisms of action. Here, we present a comprehensive study comparing the biological activities of >200 rocaglates to better understand how the presence of different chemical entities influences their biological activities. Through this, we find that most rocaglates preferentially repress the translation of mRNAs containing purine-rich 5′ leaders, but certain rocaglates lack this bias in translation repression. We also uncover an aspect of rocaglate mechanism of action in which the pool of translationally active eIF4F is diminished due to the sequestration of the complex onto RNA.

In Brief

*Correspondence: porco@bu.edu (J.A.P.), jerry.pelletier@mcgill.ca (J.P.).

AUTHOR CONTRIBUTIONS

J.C., W.Z., J.A.P., and J.P. conceived and designed the study. J.C., W.Z., R.C., F.R., W.G.D., A.S., and L.E.B. acquired, analyzed, and interpreted the data. W.C.M. and T.H. provided essential reagents. P.B.F.O. and P.V.B. provided the bioinformatic analysis. J.C. and J.P. wrote the manuscript. All of the authors commented on, edited, and approved the manuscript.

DECLARATION OF INTERESTS

J.C., W.Z., J.A.P., and J.P. have filed a US provisional patent application on the use of amidino- and amino-rocaglates as novel translation inhibitors and anticancer agents. All other authors declare no competing interests.

SUPPLEMENTAL INFORMATION

Supplemental Information can be found online at https://doi.org/10.1016/j.celrep.2020.02.002.

Rocaglates are a diverse family of small molecules that inhibit eIF4A. Chu et al. undertake a comparative analysis of the bioactivity of >200 rocaglates and uncover nuances in their mechanisms of action. Rocaglates interfere with eIF4F release from the cap and exert a bystander effect to inhibit translation.

Graphical Abstract

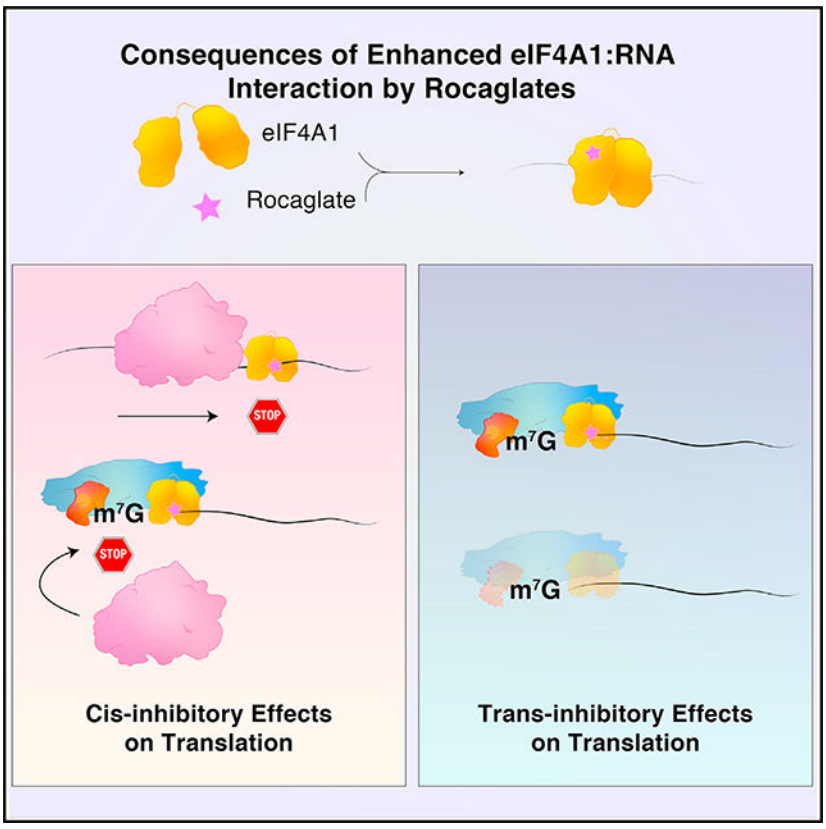

INTRODUCTION

Translation is an essential process that enables cells to make rapid and spatiotemporal alterations to the proteome, and its regulation is critical to a wide variety of biological processes, including growth, differentiation, and development. Much of translation regulation is imposed at the initiation phase, which is an intricate process involving the coordination of multiple factors. In the canonical mechanism of initiation, eukaryotic initiation factor (eIF) 4F (comprised of eIF4A, 4E, and 4G) binds to the mRNA 5′ m^7GpppN cap to facilitate the recruitment of 43S pre-initiation complexes (PICs; 40S ribosomal subunit and associated factors). The 43S PIC then scans the mRNA 5′ leader in search for an initiation codon. Structural barriers within the 5′ leader can affect the dependency of an mRNA on eIF4F and consequently influence its ability to recruit or alter the scanning efficacy of a 43S PIC (Pelletier and Sonenberg, 2019).

Targeting translation initiation has been recognized as a promising therapeutic strategy as it is frequently usurped in disease and manipulation of this process can achieve selective changes in gene expression. Of particular interest are a family of compounds collectively known as rocaglates that stabilize eIF4A:RNA interactions. Rocaglamide A (Roc A) causes eIF4A to preferentially clamp onto RNA purine-rich regions, and when this occurs within 5′ leader regions, the stabilized eIF4A:RNA complex is thought to impede 43S PIC scanning (Iwasaki et al., 2016, 2019). However, purine content was not identified as a sensitizing element in two other ribosome-profiling studies using the related rocaglate member silvestrol (Rubio et al., 2014; Wolfe et al., 2014). Instead, 5′ leaders with long, structured sequences, the presence of G-quadruplexes, and low overall GC content were identified to be most significant. Whether this discrepancy can be attributed to the fact that different rocaglate entities were used in these studies is unknown, and if so, it raises the question of whether all rocaglates operate through a shared mechanism of action.

Over 100 rocaglates have been either isolated from natural sources or synthetically derived, and limitations in accessing specific structural entities have led to laboratories using different molecules for their biological studies. In addition to Roc A and silvestrol, commonly used rocaglates include CR-1–31-B, FL3, RHT, and SDS-1–021 (Figure S1A). In this study, we address the question of whether universal conclusions can be drawn across the rocaglate family. To this end, we characterize the biological activities of >200 rocaglates. In general, we find a strong correlation between the ability of a rocaglate to stimulate the binding of eIF4A1 to RNA and their ability to inhibit translation. However, there were clear outliers suggesting that the presence of specific chemical groups within rocaglates can differentially modulate eIF4A activity, and caution must be taken when formulating global generalizations across all rocaglate family members. We also expand our understanding of the mechanism of action of rocaglates and show that they can stabilize the eIF4F complex at the cap structure, exerting two previously unappreciated consequences on the initiation process: (1) direct inhibition of translation of the target mRNA and (2) a bystander effect on mRNAs whose sequences are not directly targeted by rocaglates.

RESULTS

Rocaglate-Induced eIF4A1:RNA Clamping Is Not a Universal Predictor of Translation Inhibition Potency

We have amassed a collection of >200 synthetic rocaglates and used this unique resource to characterize their activity as translation inhibitors *in vitro* by using Krebs-2 translation extracts to assess their ability to induce eIF4A1:RNA complexes with FAM-labeled r(AG)$_8$ RNA (Iwasaki et al., 2016). Overall, the stimulation of eIF4A:RNA association correlates with inhibition of cap-dependent translation *in vitro* (Figure 1A). However, silvestrol and two synthetic silvestrol derivatives (WGD-57–590 and WGD-57–591) deviate from this trend, as these compounds exhibited relatively weak activity in the fluorescence polarization (FP) assay, yet strongly inhibited cap-dependent translation (Figures 1A and S1B). We also noted compounds that were potent at inducing eIF4A1:RNA binding but showed weak activity toward cap-dependent translation *in vitro* (Figures 1A, pink box, and S1C). Among these were two *cis*-diol-containing rocaglaols, CMLD011166 and CMLD011167. This

analysis also uncovered a potent new class of rocaglates, amidino-rocaglates (Figure 1A, yellow oval), whose characterization was recently reported (Chu et al., 2019; Zhang et al., 2019).

All of the rocaglates tested had a bias for polypurine-containing RNAs over polypyrimidine substrates (Figures 1B and S1D; Table S1). In contrast, pateamine A, a structurally unrelated eIF4A inhibitor, induced eIF4A binding to all of the RNA substrates tested (Figure S1D). All rocaglate-induced eIF4A1:poly r$(AG)_8$ complexes were significantly more stable in the presence of the non-hydrolyzable ATP analog adenosine-5'-[(β,γ)-imido] triphosphate (AMP-PNP) than in the presence of ATP (Figure S1E), as previously reported for eIF4A1:RocA:poly r$(AG)_8$ (Iwasaki et al., 2016).

Rocaglates Show Differing mRNA-Targeting Spectra in Translation Assays

The *in vitro* translation experiments described above were performed at a fixed rocaglate concentration (2 μM) using a generic bicistronic mRNA reporter (Novac et al., 2004). To better evaluate the consequences of eIF4A:polypurine clamping, we designed a series of reporters harboring cap-proximal polypurine tracks of varying lengths (Figure 1C). Through this, we observed that 5x (AG) was sufficient to elicit maximum inhibition of cap-dependent translation by CR-1–31-B (Figure 1C).

We next tested the translational response of mRNA reporters with cap-proximal $(AG)_{10}$ or $(UC)_{10}$ sequences in the presence of select rocaglates (Figure 1D). CR-1–31-B and Roc A selectively inhibited cap-dependent translation of the $(AG)_{10}$-containing reporter (Figure 1D). Unexpectedly, silvestrol and WGD-57–591 equally inhibited both mRNA reporters (Figure 1D), even though they do not stimulate the binding of recombinant eIF4A1 to polypyrimidine RNA (Figures 1B and S1D). The rocaglaol derivative CMLD011167 failed to inhibit either reporter (Figure S2A), which is consistent with its apparent lack of *in vitro* activity in the previous experiments (Figure 1A). The unrelated eIF4A inhibitors hippuristanol and pateamine A equally repressed cap-dependent translation from both reporters, demonstrating that purine selectivity in translation inhibition is not shared among all eIF4A-targeting molecules (Figure S2A).

The difference in the mRNA targeting spectrum observed between CR-1–31-B and silvestrol was not restricted to cap-proximal polypurine tracks, but was also observed with reporters where the polypurine-polypyrimidine tracks were situated 15 nt downstream of the cap, although here, the $(AG)_{10}$ reporter appeared more responsive to silvestrol than the $(UC)_{10}$ reporter (Figure S2B). Positioning a polypurine track within the 3′ UTR did not sensitize the translation to CR-1–31-B, indicating that the influence of purine richness is 5′ leader dependent (Figure S2C).

To complement the results obtained by FP, we examined the RNA-binding activity of eIF4A using biotinylated RNA pull-downs (RPDs) in translation extracts. This was undertaken to evaluate whether rocaglates induced preferential association of eIF4A1 to polypurine templates in the presence of other initiation factors and competing RNA-binding proteins. In these experiments, 30-nt biotinylated RNA baits harboring a polypurine $(AG)_{10}$ or polypyrimidine $(UC)_{10}$ track were added to translation extracts in the presence or absence of

rocaglate, followed by purification using streptavidin beads. RPDs performed with CR-1–31-B or Roc A showed that eIF4A1 was selectively associated with the purine-rich template (Figure S3A). Unlike the results obtained in the FP experiments, RPDs using rabbit reticulocyte lysates showed that silvestrol stabilizes eIF4A1 onto both the polypurine and polypyrimidine baits (Figure S3A). The bias in eIF4E retention on a polypyrimidine versus polypurine substrate may reflect a preferential sequence specificity of eIF4G for oligo-(U) sequences, as previously reported (Zinshteyn et al., 2017). Retention of eIF4A1 by silvestrol but not CR-1–31-B on polypyrimidine RNA was also observed when an ApppG-capped RNA substrate was used (Figure S3B). When the RPDs were performed using purified eIF4A1 or eIF4F, no increase in eIF4A1:polypyrimidine RNA association was observed with silvestrol (Figure S3C). These results suggest that an additional co-factor present in translation lysates is likely required to stimulate eIF4A1 binding to pyrimidine sequences in the presence of silvestrol. Because eIF4A activity is stimulated when associated with the accessory factor eIF4H, we assessed whether eIF4H would influence eIF4A RNA binding in response to silvestrol. The RPD performed using equimolar concentrations of eIF4A1 and eIF4H showed an increased retention of eIF4A1 onto the polypyrimidine RNA bait in the presence of silvestrol, but not CR-1–31-B (Figure S3D). These results suggest that eIF4A-interacting partners may influence the RNA-targeting spectrum of rocaglates. Current experiments seek to better define this phenomenon.

In Cellula Activity of Rocaglates

In addition to comparative assays *in vitro,* evaluation for bioactivity against NIH 3T3 cells was conducted with all rocaglates. To assess whether any compounds in our collection acted in an eIF4A-independent manner, cytotoxicity was also measured in the CRISPR-modified NIH 3T3 cell line eIF4A1^{em1JP}, which harbors the rocaglate-resistant eIF4A1(F163L) allele (Chu et al., 2016). We identified 13 compounds that induced >70% cell death relative to vehicle-treated cells when tested at 40 nM (Table S1). CMLD011166 and CMLD011167, which were inactive *in vitro* (Figure 1A), ranked highly among all of the compounds tested with respect to cytotoxic activity (Table S1). In contrast, WGD-57–590 and WGD-57–591, which were highly active in the *in vitro* translation experiments, were found to be weakly cytotoxic. All of the cytotoxic rocaglates showed little or significantly diminished activity toward the eIF4A1^{em1JP} cell line, indicating that eIF4A1 on-target engagement is critical to the observed phenotypic response (Figure 2A; Table S1).

To address whether differences in behavior among rocaglates toward the $(AG)_{10}$ and $(UC)_{10}$ reporters observed *in vitro* extended *in cellula,* we transfected the mRNA reporters into 293T cells and measured the relative production of luciferase in the presence of compound (Figure 2B). CR-1–31-B showed a preference for inhibiting the translation of $(AG)_{10}$-FF-HCV-Ren over $(UC)_{10}$-FF-HCV-Ren mRNA (Figure 2B), although the differences were not as pronounced as what was observed *in vitro* (Figure 1D). However, silvestrol and WGD-57–591 inhibited both reporters equally (Figure 2B). CMLD011167 demonstrated a behavior that mirrored CR-1–31-B, with a clear preference for inhibiting $(AG)_{10}$-FF-HCV-Ren mRNA (Figure 2B). The unrelated eIF4A inhibitors pateamine A and hippuristanol inhibited both reporters equally (Figure 2C).

Next, we used enhanced crosslinking immunoprecipitation (eCLIP) to determine whether we could identify instances of altered eIF4A1 clamping to endogenous cellular mRNAs. To facilitate these experiments, we introduced a 3xFLAG tag into the N terminus of the endogenous eIF4A1 using CRISPR-Cas9-mediated gene editing in 293T cells (Figure S4A). IP experiments using an anti-FLAG antibody demonstrated that the tagged eIF4A1 molecule associates with eIF4E and eIF4G (Figure S4B). Cells were exposed to vehicle, CR-1–31-B (20 nM), or silvestrol (20 nM) for 1 h, and changes to the FLAG-eIF4A1:RNA-binding landscape were determined via eCLIP. Approximately 20%–30% of the unambiguously mapped reads aligned to the 5′ leader regions, which represents a 2-fold enrichment relative to input (Figure S4C). As expected for a translation initiation factor, eIF4A1 eCLIP read density was enriched before the initiation codon (Figure S4D). In line with the “clamping” model, we observed a negative correlation between mRNAs whose 5′ leaders displayed increased eIF4A1 binding in the presence of silvestrol and previously published ribosome-profiling datasets identifying silvestrol-responsive mRNAs (Figure S4E). The absence of ribosome-profiling data for CR-1–31-B prevented us from performing the same analysis with CR-1–31-B. Overall, the changes in eIF4A1 RNA binding induced by CR-1–31-B and silvestrol were largely similar, with both compounds displaying a bias toward purine-rich motifs (orange) and a bias against “AT”-rich motifs (dark blue) (Figure 2D). We observed that “AGT”-containing motifs were more enriched in the CR-1–31-B-treated samples compared to silvestrol (Figure 2D, cyan; Table S2). Moreover, a number of differentially targeted transcripts were identified (Figure S5). For example, JUN showed a higher number of 5′ leader read counts in cells treated with CR-1–31-B compared to silvestrol (Figure S5A). The inverse was observed with PCDH9, ACTR2, and CTNND1 (Figures S5B–S5D). We then assessed whether these differences in eIF4A1 RNA binding correlated with changes in translational efficiency using polysome fractionation. We found that the translation of JUN was more affected by CR-1–31-B than by silvestrol (Figure S5A). Conversely, CTNND1 displayed a higher degree of association with eIF4A1 in the presence of silvestrol and is affected more by silvestrol compared to CR-1–31-B (Figure S5D). PCDH9 and ACTR2 were similarly responsive to both compounds (Figures S5B and S5C). While it appears that enrichment of eIF4A1 at the mRNA 5′ leader correlates with inhibition in translation, we noticed that this was not always the case. For instance, TAOK2 showed an increased accumulation of eCLIP reads with both rocaglates, yet its translation was not profoundly affected by either rocaglate when assessed by polysome fractionation (Figure S5E). Overall, these results indicate that increased eIF4A1:RNA binding represents one important aspect of determining rocaglate sensitivity, but it is by no means the only factor in play.

Rocaglates Sequester eIF4F onto RNA

As eIF4A is a critical component of the eIF4F complex, we inquired as to whether rocaglates affected the association of eIF4F toward RNA. When RPDs were performed using m^7G-capped polypurine RNA baits, the increased retention of eIF4E, eIF4A, and eIF4G was observed in the presence of rocaglates (Figure 3A). We then measured the stability of eIF4F on RNA in the presence of competitor RNA (Figure 3B). In the absence of compound, the eIF4F complex is not efficiently retained on the RNA ($t_{1/2} < 2$ min), but in the presence of CR-1–31-B, a significant proportion of eIF4E and eIF4A remains associated

with the bait RNA up to 10 min following the addition of the competitor (Figure 3B). The increased eIF4F residence time on the polypurine RNA in the presence of rocaglate is longer than the rates of translation initiation (median < 1 min) (Shah et al., 2013; Yan et al., 2016). To assess whether the rocaglate-induced trapping of eIF4F leads to translation inhibition, we pre-assembled eIF4F/CR-1 −31-B/m^7GpppG$(AG)_{10}$-FF-HCV-Ren complexes and added these to rabbit reticulocyte lysate (RRL) translation extracts. Upon doing so, we found that the mRNAs associated with a rocaglate-stabilized eIF4F complex were less efficiently translated (Figure 3C).

We hypothesized that prolonged retention of eIF4F on mRNA may deplete the limited eIF4F pool available for ribosome recruitment and lead to a *trans*-inhibitory effect toward mRNAs that are not directly affected by clamping. To test this, we programmed *in vitro* translation reactions with the $(UC)_{10}$ reporter, which is not responsive to CR-1–31-B or Roc A (Figure 1D), and added 25-fold molar excess of m^7GpppG-$(AG)_{10}$ or ApppG-$(AG)_{10}$ competitor RNA to the reaction (Figure 3D). The addition of m^7GpppG-$(AG)_{10}$ competitor sensitized m^7GpppG$(UC)_{10}$-FF-HCV-Ren mRNA to inhibition by CR-1–31-B and Roc A (Figure 3D). In contrast, the addition of ApppG-$(AG)_{10}$ and CR-1–31-B or Roc A had little impact, demonstrating this to be a cap-dependent phenomenon (Figure 3D). Accordingly, the addition of purified eIF4F partially rescued the cap-dependent inhibition induced by CR-1–31-B or silvestrol (Figure 3E).

To further evaluate the significance of rocaglate-induced gain-of-function activity of eIF4F in cells, we reasoned that the expression of wild-type (WT) eIF4A1 in eIF4A1^{em1JP} cells should resensitize these cells to rocaglates. To test this, NIH 3T3 and eIF4A1^{em1JP} cells were transduced with an empty murine stem cell virus (MSCV) cassette, MSCV/His_6-eIF4A1, or MSCV/His_6-eIF4A1(F163L) (Figure 4A). NIH 3T3 cells overexpressing WT eIF4A1 or eIF4A1(F163L) were similarly sensitive to rocaglates, and few differences were noted among them (Figure 4B). However, the expression of WT eIF4A1 in eIF4A1^{em1JP} cells significantly resensitized these to all of the tested rocaglates (Figure 4B). Overall, these results are consistent with the notion that rocaglates exert their effects by imparting a gain-of-function activity to eIF4A1.

DISCUSSION

A surprising revelation of this study is that rocaglates can exert different effects on gene expression. While the degree of eIF4A1 stabilization onto RNA was generally a good predictor of the extent of translation inhibition, there were clear outliers to this trend. We also found differences between rocaglates in their mRNA-targeting preference. CR-1–31-B and Roc A preferentially inhibited purine-rich mRNAs, whereas this bias was diminished with compounds like silvestrol (Figures 1D and 2B). Silvestrol, WGD-57–590, and WGD-57–591 are the only molecules within the collection containing a 1,4-dioxanyloxy moiety, and these compounds inhibited translation *in vitro* far more potently than what could be predicted based on their relatively weak ability to stimulate eIF4A1:RNA association (Figure 1A; Table S1). eCLIP experiments revealed that although the situation is more complex with cellular mRNAs, there were distinct biases uncovered between CR-1–31-B and silvestrol (Figure 2D).

Our results also suggest that interacting partners of eIF4A1 may play a role in rocaglate response. While RPDs performed from cell-free translation systems showed that silvestrol was able to stimulate eIF4A1 association onto poly r(UC)$_{10}$, this effect was not observed in RPDs using recombinant eIF4A1 or purified eIF4F (Figure S3B). However, the addition of eIF4H to RPDs using recombinant eIF4A1 yielded results similar to the RPDs performed with the translation extracts, suggesting that co-factors can modulate the eIF4A1 response toward rocaglates. It would be of interest to assess whether other eIF4A-associating proteins, such as eIF4B, are capable of exerting effects similar to eIF4H.

Another class of outliers included CMLD011166 and CMLD011167, which are the only compounds in our collection with a *cis*-1,2-cyclopentanediol core. In spite of their potent ability to stimulate eIF4A1:RNA association, the *cis*-diol rocaglaols did not inhibit translation in *in vitro* cell-free translation systems. Nevertheless, these compounds are able to block translation in cells and are highly cytotoxic (Table S1). The mechanism of action of the *cis*-diol rocaglaols is also eIF4A1 dependent since cells harboring the eIF4A1 F163L mutation were resistant. Our results caution against generalizations attributing specific mRNA-responsive features to all biologically active rocaglates.

The additional mechanisms of action by rocaglates found in this work complement the recently proposed clamped-barrier model (Figure 4C). As reported, rocaglates can stabilize eIF4A to 5′ leader regions and block 43S scanning (Figure 4C, step 1) (Iwasaki et al., 2016). However, this mechanism does not fully encapsulate the global changes in mRNA translation that are induced by rocaglates. Our data indicate a more complex mechanism of action, as we found that rocaglates can also trap eIF4F complexes at the cap (Figure 3). This is associated with reduced translation and is likely due to diminished 43S PIC recruitment to the targeted mRNA (Figure 4C, step 2). eIF4E has been shown to influence eIF4A-mediated mRNA restructuring (Feoktistova et al., 2013), and a potential impact of eIF4E on rocaglate-response remains to be evaluated. By extending the resident time of eIF4F at the cap (Figure 3B), rocaglates can also exert a bystander effect that leads to *trans*-inhibition of translation on otherwise normally unresponsive mRNAs (Figure 4C, step 3). As this effect is rescued by the addition of eIF4F, we surmise that it results from a decrease in the levels of free eIF4F. In providing a better understanding of the mechanism of translation repression by rocaglates, we have begun to define the nuances and complexities that this class of compounds exerts on gene expression.

STAR★METHODS

LEAD CONTACT AND MATERIALS AVAILABILITY

Further information and requests for resources and reagents generated in this study should be directed to and will be fulfilled by the Lead Contact, Jerry Pelletier (jerry.pelletier@mcgill.ca). All unique/stable reagents generated in this study are available from the Lead Contact with a completed Materials Transfer Agreement.

EXPERIMENTAL MODEL AND SUBJECT DETAILS

Cell Culture—All cell lines used in this study were maintained in DMEM supplemented with 10% FBS (Wisent), 100 U/mL penicillin/streptomycin, and 2 mM L-glutamine at 37°C and 5% CO_2. Details describing the generation of the CRISPR-modified NIH/3T3 line, eIF4A1^{em1jp} can be found in a prior publication (Chu et al., 2016)

METHOD DETAILS

Compounds—Rocaglates were synthesized using ESIPT photocycloaddition of 3-hydroxyflavones with cinnamates as previously reported, followed by further functionalizations (Rodrigo et al., 2012; Stone et al., 2015; Yueh et al., 2017). A few compounds are present more than once in the collection and arose from different synthesis batches or the preparations contain two enantiomers (see Table S1). Compounds were resuspended in DMSO to a final concentration of 10 mM and stored at −80°C.

Recombinant DNA Constructs—Plasmids expressing the $(AG)_{10}$- and $(UC)_{10}$-reporters were constructed through modification of pKS-FF-HCV-Ren vector (Novac et al., 2004). To facilitate the replacement of 5′ leader sequences, MluI and NdeI restriction sites were introduced upstream of the T3 promoter and of the FF AUG start codon, respectively. These sites were added as part of G blocks and cloned into the pKS-FF-HCV-Ren vector using PciI and NarI restriction sites. Different 5′ leader sequences were then introduced to the reporters by annealing two overlapping phosphorylated oligonucleotides with the desired sequences, and directionally cloned into the vector using the engineered MluI and NdeI restriction sites.

Cell Culture and Retroviral Transduction—All cell lines used in this study were maintained in DMEM supplemented with 10% FBS (Wisent), 100 U/mL penicillin/streptomycin, and 2 mM L-glutamine at 37°C and 5% CO_2. For overexpression studies with eIF4A1 in NIH/3T3 or eIF4A1^{em1jp} cells, ecotropic Phoenix cells were first transfected with retroviral vectors expressing codon optimized His_6-tagged eIF4A1 (WT or F163L). Forty-eight hours post-transfection, the viral supernatant was harvested, filtered, and added to NIH/3T3 or eIF4A1^{em1jp} cells in the presence of 4 μg/mL polybrene once every 12 h for a total of 4 infections. Two days after the final infection, cells were seeded for SRB assays (described below) and western blotting.

CRISPR/Cas9 Mediated Gene Editing—A guide sequence overlapping the translation start codon of eIF4A1 ($^{5'}$GACATGATCCTTAGAAACTA$^{3'}$) and complementary to the DNA coding stand (Figure S4A) was cloned into an all-in-one LeGO-based vector expressing Cas9-D10A. A donor sequence containing 900 bp homology flanking both sides of the 3X FLAG sequence was synthesized by IDT and cloned into the pUC57 EcoRV site. To introduce the 3X FLAG tag into the endogenous eIF4A1 locus, 293T cells were seeded to 70% confluency in a 10 cm dish and transfected with 20 μg of donor plasmid and 10 μg of the targeting vector using calcium phosphate. The cells were refreshed with media the next day. To screen for cells containing the 3X FLAG modification, two rounds of limiting dilution were performed. For the first round, 10 cells were seeded per well in a 96 well format two days following transfection. Approximately 2 weeks after seeding, when cells approached confluency, the plate was replicated and one plate evaluated using

immunofluorescence (IF) with anti-FLAG antibody (Sigma, F1804). Wells that contained cells that were positive for 3X FLAG eIF4A1 (as determined by IF) were expanded and then seeded for a second round of limiting dilution, in which one cell was seeded per well in a 96 well format. The presence of successful homologous recombination as well as homogeneity of cell line was evaluated using immunofluorescence.

Immunofluorescence—Cells were first washed with PBS and then fixed using 3.7% freshly prepared paraformaldehyde for 15 min at room temperature. Afterwards, the cells were washed twice with PBS and then permeabilized with 0.3% Triton X-100 in PHEM (60 mM PIPES [pH 7.2], 25 mM HEPES, 10 mM EGTA, 4 mM $MgSO_4$) for 10 min at room temperature and then washed with PBS. The cells were then blocked with 5% goat serum in PHEM for 1 h at room temperature. To detect FLAG peptides, monoclonal anti-FLAG antibody (Sigma, F1804) was prepared at a 1:1000 dilution in 5% goat serum/PHEM and then incubated overnight with the fixed cells at 4°C. The cells were washed 5 times with PBS (10 minutes between washes) before incubation with secondary antibody coupled to Alexa Fluor 594. Incubation was performed at room temperature for 1 h and the cells were then washed 5 times with PBS (10 minutes per wash). During the second PBS wash, the cells were counterstained with DAPI (1:10000 in PBS).

Co-immunoprecipitation Experiments—Parental 293T or 3xFLAG-eIF4A1 293T cells were lysed with a buffer containing 50 mM HEPES [pH 7.5], 150 mM KCl, 2 mM EDTA, 0.5% NP-40, 1mM NaF 1 1mM PMSF, 4 μg/mL aprotinin, 2 μg/mL leupeptin, and 2 μg/mL pepstatin. Lysates were cleared via centrifugation and protein concentrations were determined using a DC assay (Bio-Rad). For each sample, 30 μl of anti-FLAG magnetic beads (Sigma, M8823) was washed twice with lysis buffer and then added to 500 μg lysate. The beads were incubated end-over-end with the lysates for 1 h at 4°C and then washed 3 times with lysis buffer (each wash was incubated for 10 minutes at 4°C). Proteins were eluted from the beads through the addition of 1X SDS sample buffer and analyzed using immunoblotting.

Purification of Recombinant Proteins—pET15b-His_6-eIF4A1 was transformed into BL21 (DE3) bacteria, plated onto LB-Agar plates, and single colonies were used to inoculate an overnight starter culture in LB containing 100 mg/L ampicillin. This culture was expanded the following day at a 1:50 dilution, and the bacteria was further cultured at 37°C until the OD_{600} reached 0.6–0.8. At this point, the cultures were induced with 1mM IPTG and grown for an additional 3 h. The bacteria was pelleted and resuspended in buffer containing 20 mM Tris [pH 7.5], 10% glycerol, 0.1 mM EDTA, 200 mM KCl, 0.1% Triton X-100, 3.4 mM β-mercaptoethanol. Cells were lysed via sonication and cellular debris were cleared via centrifugation. The cleared lysates were supplemented with 20 mM imidazole and then loaded onto a Ni-NTA agarose column (QIAGEN). The column was washed 3 times with 4 column volumes of wash buffer 1 (20 mM Tris [pH 7.5], 10% glycerol, 0.1 mM EDTA, 800 mM KCl, 20 mM imidazole), followed by 3 washes using 4 column volumes of wash buffer 2 (Wash buffer 1 containing 300 mM KCl). Purified proteins were eluted with wash buffer 2 containing 200 mM imidazole. The eluate was dialyzed overnight in buffer containing 20 mM Tris [pH 7.5], 10% glycerol, 0.1 mM EDTA, 100 mM KCl, and 2 mM

DTT. The next day, the dialyzed samples were subjected to further purification through a Q-Sepharose Fast Flow (Amersham) column, and eluted with a 100 mM-500 mM KCl gradient in 20 mM Tris [pH 7.5] 10% glycrerol and 0.1 mM EDTA. The final dialysis was performed in a buffer containing 20 mM Tris [pH 7.5], 10% glycerol, 0.1 mM EDTA and 2 mM DTT.

In Vitro* Translation Assays—In vitro* translation assays performed in Krebs-2 cell extracts with the addition of 5 mM $MgCl_2$,30 mM Tris-HCl [pH 7.5], 1.5 mM ATP, 0.1mM GTP, 0.6mM CTP, 10mM dipotassium creatine phosphate, 80 μg/mL creatine kinase, and 0.04 mM amino acids. The *in vitro* transcribed mRNA reporters were added to the Krebs-2 extracts to a final concentration of 10 ng/μl and incubated for 60 min at 30°C prior to the measurement of luciferase activities.

Fluorescence Polarization Assays—Unless otherwise specified, 500 nM recombinant eIF4A1 was added to 10 nM FAM-labeled RNA in a buffer containing 14.4 mM HEPES-NaOH [pH 8], 108 mM NaCl, 1mM $MgCl_2$,14.4% glycerol, 0.1% DMSO, 2mM DTT and 1mM AMPPNP in black, low volume 384 well plates (Corning 3820). Binding reactions were allowed to equilibrate for 30 min at 22°C in the dark prior to measuring polarization values on a Pherastar FS microplate reader (BMG Labtech). For the dissociation experiments, the eIF4A:FAM-$(AG)_8$ complexes were pre-assembled in the presence of 50 μM compound, incubated at 22°C for 30 min in presence of either 1 mM ATP or AMP-PNP, at which point 100 μM unlabelled $(AG)_8$ RNA was added and measurements were performed. For conditions involving ATP and DMSO, 50 μM eIF4A was used instead of 1 μM due to the low affinity of eIF4A for RNA.

RNA Transfections—HEK293T cells were transfected in a 24 well plate with 0.25 μg/well of *in vitro* transcribed $m^7GpppG(AG)_{10}$-FF-HCV-Ren or $m^7GpppG(UC)_{10}$FF-HCV-Ren mRNA using DMRIE-C following the manufacturer's instructions (ThermoFisher, 10459014). One hour later, cells were exposed to the indicated concentrations of compounds for an additional 6 h. Following this, extracts were prepared using passive lysis buffer (PLB, Promega) and luciferase activity measured on a Berthold Lumat LB 9507 luminometer.

Sulforhodamine B (SRB) assay—One thousand cells were seeded per well in a 96 well format and then cultured in the presence of 40 nM compound (unless indicated otherwise). Cells were grown for 4 days before processing. Plates were washed with PBS, fixed with 50% cold trichloroacetic (TCA) acid for 1 h, and stained with 0.5% sulforhodamine B (dissolved in 1% acetic acid) for 15 min. The unbound dye was removed by washing the plates 5 times with 1% acetic acid. The plates were then dried, and the remaining dye was solubilized in 10 mM Tris [pH 9] before measuring OD_{510} nm values on a Spectramax M5 (Molecular Devices).

RNA Pull Down (RPD) Experiments—RNAs were synthesized via *in vitro* transcription using T7 RNA polymerase (New England Biolabs). Annealed DNA ultramers (Integrated DNA Technologies) served as templates. Biotin-11-UTP or Biotin-11-ATP (Perkin Elmer) were added at a final concentration of 0.1 mM (which is 10-fold less relative to unmodified NTPs) to the *in vitro* transcription reactions to generate biotinylated $(AG)_{10}U_{10}$ or $(UC)_{10}A_{10}$, respectively. Rabbit reticulocyte lysates (Promega) were pre-incubated with 500

nM of the indicated compound for 15 min at 30°C prior to the addition of m^7GpppG- or ApppG-capped biotinylated RNAs (added to a final concentration of 1 μM biotinylated RNA bait). Reactions were incubated for an additional 15 min at 30°C and then diluted 10x with ice cold wash buffer (0.5% v/v NP-40, 50 mM HEPES [pH 7.3], 150 mM KCl, 2 mM EDTA, 2 mM $MgCl_2$, 200 μg/ml heparin). Magnetic streptavidin beads (NEB) were used to capture the biotinylated RNA baits and the reactions were incubated end over end for 1 h at 4°C. The beads were then washed three times with ice cold wash buffer (10 min per wash) and the RNA bound proteins were eluted by digesting with 50 U of RNaseI (Ambion, AM2294) for 15 min at 37°C. Eluted proteins were analyzed by western blotting.

Western Blotting—Cells were pelleted, washed with PBS and lysed with NP40 lysis buffer (150mM NaCl, 2mM EDTA, 0.5% NP40, 20mM Tris (pH 7.3), 1mM PMSF, 4 μg/mL aprotinin, 2 μg/mL leupeptin, 2 μg/mL pepstatin). The cellular debris was pelleted by centrifugation at 16000 x *g* for 5 min and the protein concentration of the lysates was quantitated using DC assay (BioRad) according to manufacturer's instructions. The prepared lysates were then resolved on a 10% NuPAGE gel. The antibodies used for protein expression analysis were directed against eIF4A1 (Abcam, ab31217), eIF4E (Cell Signaling, #9742), eIF4G (Cell Signaling, #2498), eIF4H (Cell Signaling, #3469S), FLAG (F1804, Sigma), and eEF2 (Cell Signaling, #2332).

eCLIP—Briefly, 20 million 293T FLAG eIF4A1 cells were exposed to 0.05% DMSO, 20 nM CR-1–31-B or silvestrol for one hour prior to crosslinking (254 nm, 400 mJ/cm^2, Hoefer UVC 500). The cells were then harvested and processed as originally described in Van Nostrand et al. (2016). The only modification made to the protocol was the use of anti-FLAG M2 magnetic beads (Sigma, M8823) for the FLAG-eIF4A1 pulldown.

Polysome fractionation—HEK293T cells were exposed to vehicle, 20 nM CR-1–31-B or 20 nM silvestrol for 1 h and washed 2 times with ice-cold PBS containing 100 μg/ml cycloheximide. The cells were pelleted and washed once more prior to lysis using a hypotonic lysis buffer ((5 mM Tris-HCl [pH 7.5], 2.5mM $MgCl_2$,1.5 mM KCl, 2 mM DTT, 1% Triton X-100, 0.5% sodium deoxycholate, 100 μg/ml cycloheximide). Lysates were cleared and loaded onto a 10%–50% sucrose gradient. The gradients were centrifuged at 35000 rpm for 2 h and 15 min, then fractionated using the Teledyne ISCO Foxy R1 collector. RNA was extracted from each fraction using Trizol and cDNA was synthesized using M-MuLV reverse transcriptase (NEB, M0253L) and random hexamers (NEB, S1330S) following the manufacturer's instructions. Relative distribution of the indicated mRNAs across the polysome profile was assessed with RT-qPCR using SsoFast EvaGreen mastermix (Bio-Rad). The primer pairs used in this experiment are as follows: JUN-f ($^{5'}$ATCAAGGCGGAGAGGAAGCG$^{3'}$), JUN-r ($^{5'}$TGAGCATGTTGGCCGTGGAC$^{3'}$), ACTR2-f (^{5}GGCAGTTCTGACTTTGTACGC^{3}), ACTR2-r ($^{5'}$CCAGTCTCCTGGTAAGATGAGG$^{3'}$), CTNND1-f ($^{5'}$GTGACAACACGGACAGTACAG$^{3'}$), CTNND1-r ($^{5'}$TTCTTGCG GAAATCACGACCC$^{3'}$), PCDH9-f ($^{5'}$CTGCTCTGATTGCCTGTTTAAGG$^{3'}$), PCDH9-r ($^{5'}$ACCAGTCTGTAGACAAGGCTG$^{3'}$), TAOK2-f ($^{5'}$GGACTTTGGTTCTGCGTCCAT$^{3'}$) and TAOK-2-r ($^{5'}$TCGATGCAGGTTATCCCCAAG$^{3'}$).

eCLIP data analysis—The cDNA libraries obtained from eCLIP experiments (in 3 biological replicates for each condition) were multiplexed and sequenced to produce a dataset consisting of 900 million 50 bp paired end reads. The adaptor sequence ($5'$ AGATCGGAAGAGCGTCGTGTAG$3'$) was removed with Cutadapt (Martin, 2011). The sequencing library was demultiplexed using a custom python script (see Table S2 for barcodes). The reads were first aligned to rDNA using bowtie with (-a -v 3) parameters (Langmead et al., 2009). Approximately 40% of the reads mapped to rDNA and were removed from further analysis. The remaining reads were aligned to the RefSeq catalog of human transcripts using bowtie with (-a -m 100 -v 2) parameters which resulted in the mapping of 5%–10% of the reads (depending on the demultiplexed library). The RefSeq catalog was downloaded on 22 March 2017 from NCBI and it corresponds to version 80. Reads that ambiguously mapped to transcripts derived from different gene loci were removed using a custom python script. Mapped reads aggregated from all three replicates (ranging from 2.1 million reads to 3.8 million reads depending on the library) were used to produce plots in the figures. The $3'$ ends of reads were used to mark the positions of the reads in the alignment with an exception of when the reads were assigned to functional mRNA categories (Figure S4C) where the $5'$ end of the read was used for assigning the read location. Differential expression analysis was carried out using the Z-score approach in which genes are first binned based by lowest raw read count across the two treatments (DMSO, treated) and then log2 fold change of each gene is standardized (Andreev et al., 2015).

To produce metagene profiles relative to CDS start (Figure S4D), read densities were normalized for each transcript to avoid disproportional influence from highly abundant transcripts and the mean density values were used. For the relative enrichment of nucleotide quadruplet motifs, the regions of the transcripts from the $5'$ end to the first 30 nucleotides of the coding region were used. The log2 fold difference (treated/DMSO) for each motif frequency was normalized by the average log2 fold difference across all motifs.

QUANTIFICATION AND STATISTICAL ANALYSIS

Statistical analyses were carried out in Prism 7.0. Data represents the mean of at least 3 biological replicates ± SEM, unless indicated otherwise. All of the statistical details can be found in the figure legends.

DATA AND CODE AVAILABILITY

The accession number for the eCLIP data originating from this study is GEO: GSE142338.

Supplementary Material

Refer to Web version on PubMed Central for supplementary material.

ACKNOWLEDGMENTS

This work was supported by a Health Research Board (HRB)-Science Foundation Ireland (SFI)-Wellcome Trust Biomedical Research Partnership Investigator Award in Science (210692/Z/18/) to P.V.B., a Canadian Institutes of Health Research (CIHR) Foundation Grant (FDN-148366) to J.P., and research grants from the NIH to J.A.P. (R35 GM118173, R24 GM-111625, and R01 GM-067041).

REFERENCES

Andreev DE, O'Connor PB, Zhdanov AV, Dmitriev RI, Shatsky IN, Papkovsky DB, and Baranov PV (2015). Oxygen and glucose deprivation induces widespread alterations in mRNA translation within 20 minutes. Genome Biol. 16, 90. [PubMed: 25943107]

Chu J, Galicia-Vázquez G, Cencic R, Mills JR, Katigbak A, Porco JA Jr., and Pelletier J (2016). CRISPR-Mediated Drug-Target Validation Reveals Selective Pharmacological Inhibition of the RNA Helicase, eIF4A. Cell Rep 15, 2340–2347. [PubMed: 27239032]

Chu J, Zhang W, Cencic R, Devine WG, Beglov D, Henkel T, Brown LE, Vajda S, Porco JA Jr., and Pelletier J (2019). Amidino-Rocaglates: A Potent Class of eIF4A Inhibitors. Cell Chem. Biol. 26, 1586–1593.e3. [PubMed: 31519508]

Feoktistova K, Tuvshintogs E, Do A, and Fraser CS (2013). Human eIF4E promotes mRNA restructuring by stimulating eIF4A helicase activity. Proc. Natl. Acad. Sci. USA 110, 13339–13344. [PubMed: 23901100]

Iwasaki S, Floor SN, and Ingolia NT (2016). Rocaglates convert DEAD-box protein eIF4A into a sequence-selective translational repressor. Nature 534, 558–561. [PubMed: 27309803]

Iwasaki S, Iwasaki W, Takahashi M, Sakamoto A, Watanabe C, Shi-chino Y, Floor SN, Fujiwara K, Mito M, Dodo K, et al. (2019). The Translation Inhibitor Rocaglamide Targets a Bimolecular Cavity between eIF4A and Polypurine RNA. Mol. Cell 73, 738–748.e9. [PubMed: 30595437]

Langmead B, Trapnell C, Pop M, and Salzberg SL (2009). Ultrafast and memory-efficient alignment of short DNA sequences to the human genome. Genome Biol. 10, R25. [PubMed: 19261174]

Martin M (2011). Cutadapt removes adapter sequences from high-throughput sequencing reads. EMBnet J. 17, 10–12.

Novac O, Guenier AS, and Pelletier J (2004). Inhibitors of protein synthesis identified by a high throughput multiplexed translation screen. Nucleic Acids Res. 32, 902–915. [PubMed: 14769948]

Pelletier J, and Sonenberg N (2019). The Organizing Principles of Eukaryotic Ribosome Recruitment. Annu. Rev. Biochem. 88, 307–335. [PubMed: 31220979]

Rodrigo CM, Cencic R, Roche SP, Pelletier J, and Porco JA (2012). Synthesis of rocaglamide hydroxamates and related compounds as eukaryotic translation inhibitors: synthetic and biological studies. J. Med. Chem. 55, 558–562. [PubMed: 22128783]

Rubio CA, Weisburd B, Holderfield M, Arias C, Fang E, DeRisi JL, and Fanidi A (2014). Transcriptome-wide characterization of the eIF4A signature highlights plasticity in translation regulation. Genome Biol. 15, 476. [PubMed: 25273840]

Shah P, Ding Y, Niemczyk M, Kudla G, and Plotkin JB (2013). Rate-limiting steps in yeast protein translation. Cell 153, 1589–1601. [PubMed: 23791185]

Stone SD, Lajkiewicz NJ, Whitesell L, Hilmy A, and Porco JA Jr. (2015). Biomimetic kinetic resolution: highly enantio- and diastereoselective transfer hydrogenation of aglain ketones to access flavagline natural products. J. Am. Chem. Soc. 137, 525–530. [PubMed: 25514979]

Van Nostrand EL, Pratt GA, Shishkin AA, Gelboin-Burkhart C, Fang MY, Sundararaman B, Blue SM, Nguyen TB, Surka C, Elkins K, et al. (2016). Robust transcriptome-wide discovery of RNA-binding protein binding sites with enhanced CLIP (eCLIP). Nat. Methods 13, 508–514. [PubMed: 27018577]

Wolfe AL, Singh K, Zhong Y, Drewe P, Rajasekhar VK, Sanghvi VR, Mavrakis KJ, Jiang M, Roderick JE, Van der Meulen J, et al. (2014). RNA G-quadruplexes cause eIF4A-dependent oncogene translation in cancer. Nature 513, 65–70. [PubMed: 25079319]

Yan X, Hoek TA, Vale RD, and Tanenbaum ME (2016). Dynamics of Translation of Single mRNA Molecules In Vivo. Cell 165, 976–989. [PubMed: 27153498]

Yueh H, Gao Q, Porco JA Jr., and Beeler AB (2017). A photochemical flow reactor for large scale syntheses of aglain and rocaglate natural product analogues. Bioorg. Med. Chem. 25, 6197–6202. [PubMed: 28666859]

Zhang W, Chu J, Cyr AM, Yueh H, Brown LE, Wang TT, Pelletier J, and Porco JA Jr. (2019). Intercepted Retro-Nazarov Reaction: Syntheses of Amidino-Rocaglate Derivatives and Their Biological Evaluation as eIF4A Inhibitors. J. Am. Chem. Soc. 141, 12891–12900. [PubMed: 31310112]

Zinshteyn B, Rojas-Duran MF, and Gilbert WV (2017). Translation initiation factor eIF4G1 preferentially binds yeast transcript leaders containing conserved oligo-uridine motifs. RNA 23, 1365–1375. [PubMed: 28546148]

Highlights

- Rocaglates produce distinct inhibitory effects on translation initiation
- Rocaglates interfere with eIF4F release from the cap structure
- Rocaglates exert a bystander effect on translation initiation by sequestering eIF4F

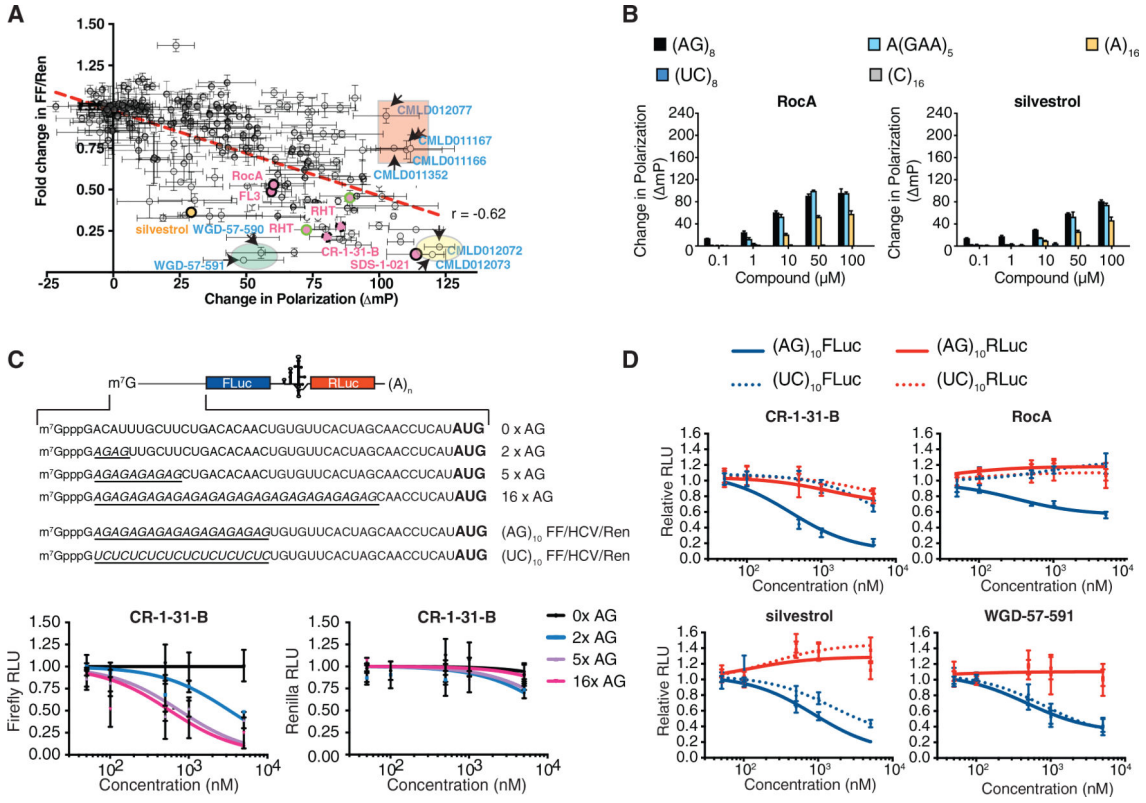

Figure 1. Different Rocaglates Exhibit Distinct Biological Activities

(A) Polypurine clamping is a correlative, but not universal, predictor of cap-dependent inhibition. The ΔmP obtained with eIF4A1:poly r(AG)8 RNA was measured for each compound (10 μM) and is plotted against the fold inhibition for cap-dependent translation (2 μM) of FF-HCV-Ren mRNA in Krebs-2. Note the duplicate values for RHT (open circles) are due to two preparations of different enantiomeric purity, and the duplicate values for CR-1–31-B (dotted circles) are due to two different compound batches (see Table S1). Pearson r = −0.62; $p < 0.0001$.

(B) Rocaglates preferentially stimulate eIF4A binding onto purine-rich RNAs. Different RNA probes were incubated in the presence of 500 nM eIF4A1 and compound for 30 min before measurement. The ΔmP in the presence of compound relative to vehicle control is presented; n = 3 ± SEM.

(C) mRNA sensitivity toward CR-1–31-B is correlated to 5′ leader purine content. The inhibition of cap-dependent (FLuc) and -independent (RLuc) translation was measured in response to CR-1–31-B; n = 3 ± SEM.

(D) Dose response of the indicated rocaglates in Krebs-2 extracts programmed with the indicated mRNAs; n = 3 ± SEM.

See also Figures S1, S2, and S3 and Table S1.

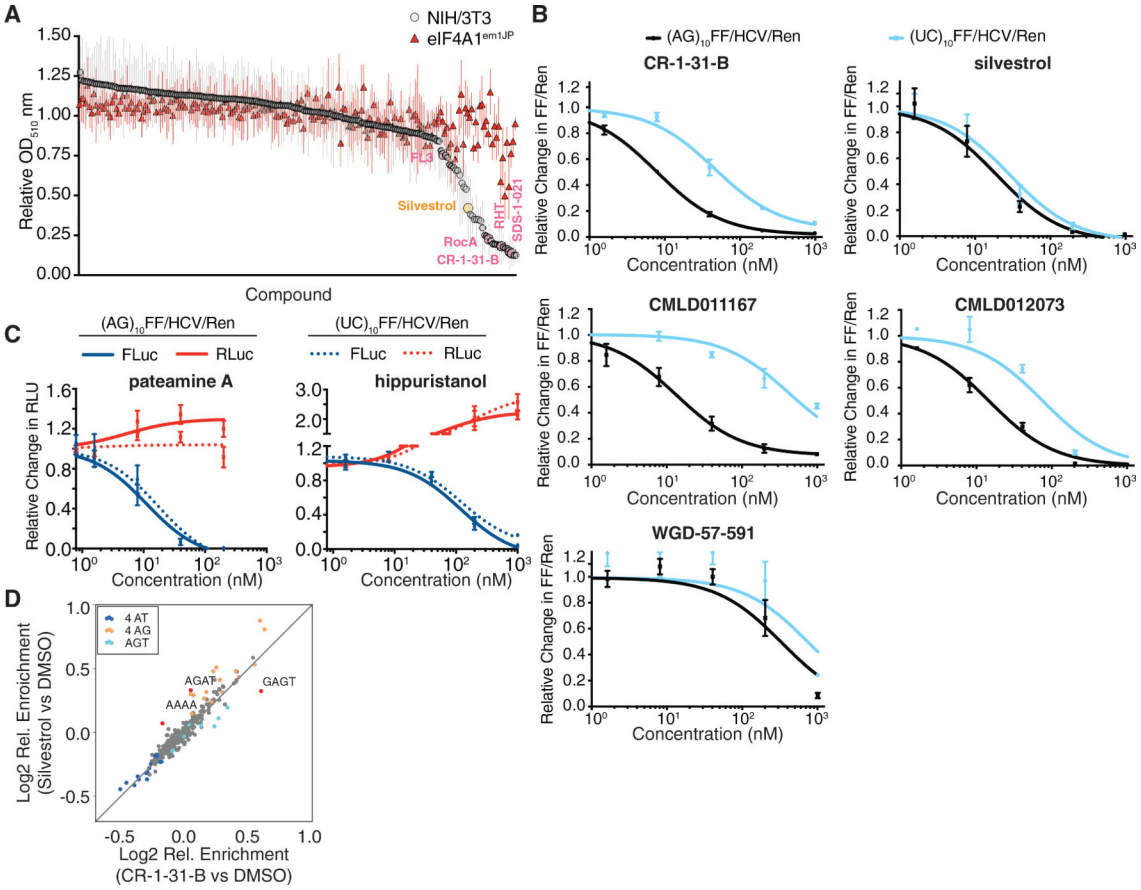

Figure 2. *In Cellula* Activity of Rocaglates

(A) Cytotoxicity of rocaglates toward NIH 3T3 (gray circle) and eIF4A1^{em1JP} (red triangle) cells. Cells were exposed to 40 nM compound for 4 days, and viability was measured using the sulforhodamine B (SRB) assay; n = 3 ± SEM.

(B) Rocaglates show different sequence preferences for inhibiting cap-dependent translation *in cellula.* HEK293T cells were transfected with the indicated mRNA reporters, compounds added 1 h later, and luciferase activity measured; n = 3 ± SD.

(C) Dose response of the indicated mRNAs to hippuristanol and pateamine in HEK293T cells; n = 3 ± SD.

(D) Comparison of the frequencies of quadruplet motifs in 5′ leaders of eIF4A1-bound mRNAs upon CR-1–13-B and silvestrol treatments relative to DMSO. The quadruplet motifs are color-coded: blue is for W4, orange is for R4, and cyan is for NAGT and AGTN. W = A, T; R = A, G. Data are compiled in Table S2.

See also Figure S4 and Table S1.

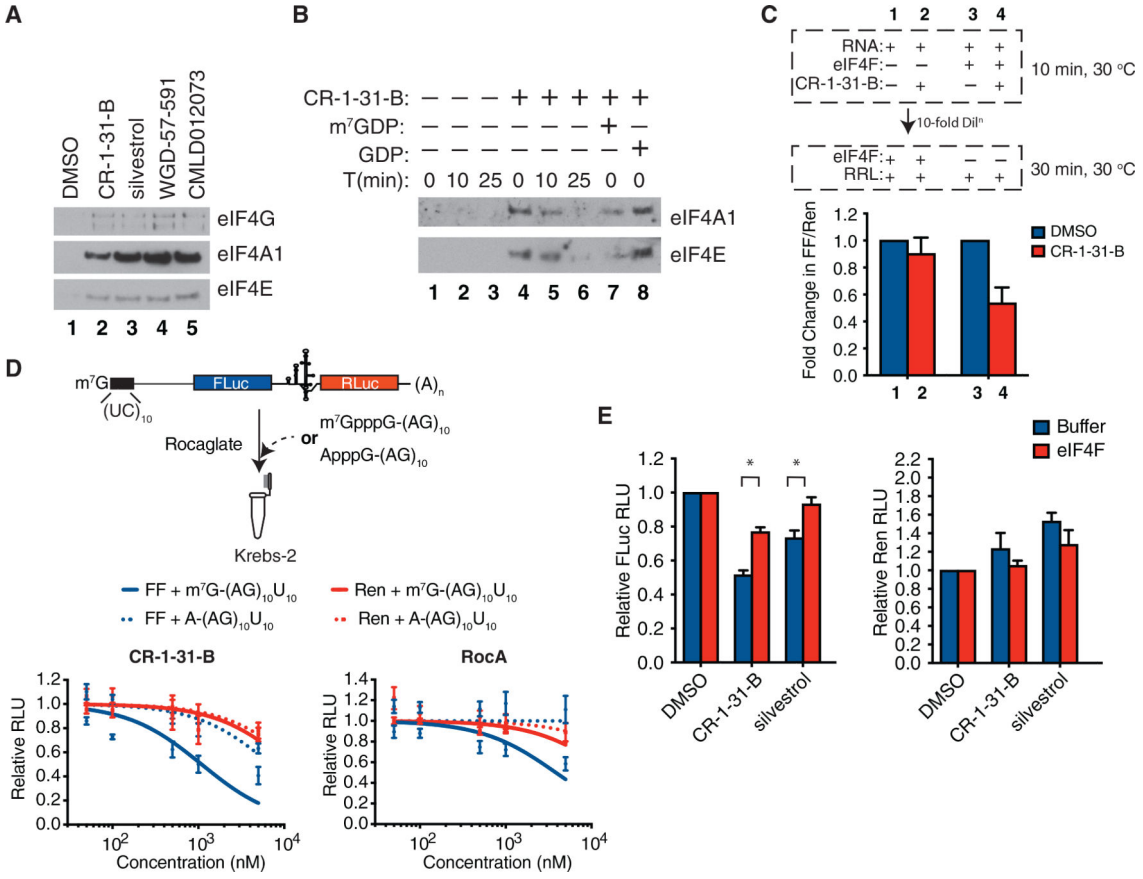

Figure 3. Increased eIF4F Retention Time on mRNA by Rocaglates Inhibits Translation

(A) RPDs performed with m^{7}GpppG-capped RNA in RRL with DMSO or 500 nM rocaglate.

(B) eIF4F:RNA complexes are stabilized by rocaglates. Biotinylated m^{7}GpppG-capped polypurine RNA (1 μM) was incubated in the presence of purified eIF4F (4 nM) in the presence or absence of CR-1–31-B (500 nM). A 10-fold molar excess of non-biotinylated RNA was then added to the reaction for the indicated periods of time before the streptavidin pull-down. Complexes retained on the biotinylated RNA were then assessed by immunoblotting.

(C) eIF4F pre-stabilized onto m^{7}GpppG(AG)$_{10}$-FF-HCV-Ren by CR-1–31-B represses cap-dependent translation. RNA (100 nM), eIF4F (100 nM), and CR-1–31-B (500 nM) were pre-incubated at 30°C for 10 min and then added to RRL translation extracts.

(D) The presence of m^{7}GpppG-capped but not ApppG-capped purine-rich RNAs sensitizes the RocA/CR-1–31-B-unresponsive m^{7}GpppG(UC)$_{10}$-FF-HCV-Ren mRNA reporter. Translation reactions were performed in Krebs-2 extracts with 10 nM mRNA reporter and 250 nM competitor RNA; n = 3 ± SEM.

(E) Addition of purified eIF4F rescues rocaglate-mediated translation inhibition. The m^{7}GpppG(AG)$_{10}$-FF-HCV-Ren reporter was added to Krebs-2 translation extracts in the presence of eIF4F (10 nM) and 100 nM of the indicated compound; n ≥ 3 ± SEM.

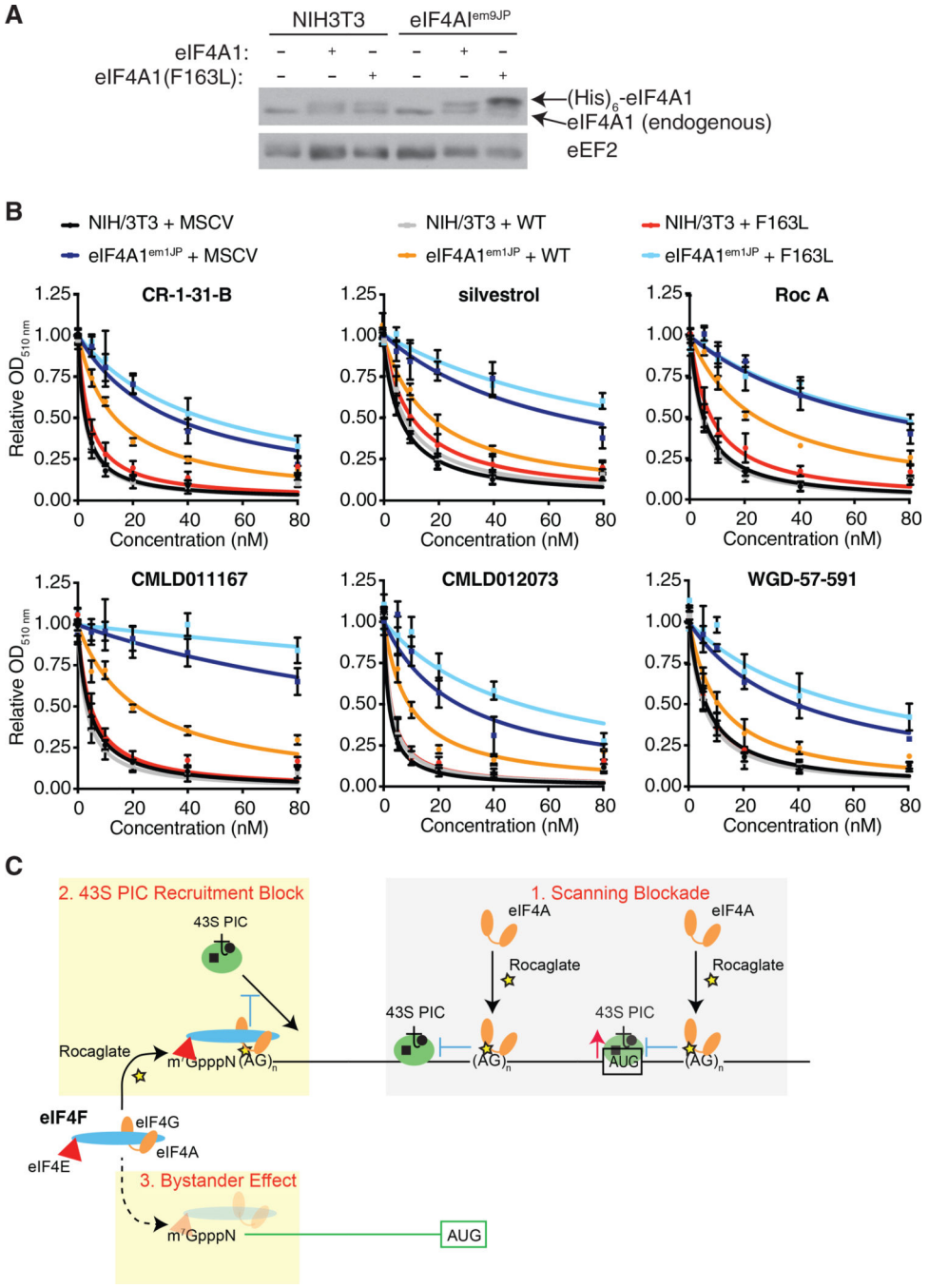

Figure 4. Rocaglates Function through a Conditional Gain-of-Function Mechanism

(A) Western blot documenting endogenous and ectopic eIF4A1 levels.

(B) Ectopic expression of WT eIF4A1 sensitizes rocaglate-resistant cells to cell death. NIH 3T3 or eIF4A1^{em1JP} cells were infected with an empty MSCV cassette or by expressing either WT eIF4A1 or eIF4A1(F163L). Viability was assessed following a 4-day exposure to 40 nM of compound using SRB assays; n = 3 ± SEM.

(C) Schematic diagram highlighting the different ways by which rocaglates target translation.

KEY RESOURCES TABLE

REAGENT or RESOURCE	SOURCE	IDENTIFIER
Antibodies		
FLAG	Sigma	Cat#: F1804
eIF4A1	Abcam	Cat#: ab31217
eIF4E	Cell Signaling	Cat#: 9742
eIF4G	Cell Signaling	Cat#: 2498
eIF4H	Cell Signaling	Cat#: 3469S
eEF2	Cell Signaling	Cat#: 2332
Bacterial and Virus Strains		
E.coli BL21(DE3)pLys	Promega	Cat#: L1195
E.coli DH10B	New England Biolabs	Cat#: C3019I
Chemicals, Peptides, and Recombinant Proteins		
Cycloheximide	Sigma-Aldrich	Cat#: C7698-5G
Sulforhodamine B sodium salt	Sigma-Aldrich	Cat#: S1402-5G
T3 RNA polymerase	New England Biolabs	Cat#: M0378S
T7 RNA polymerase	New England Biolabs	Cat#: M0251L
m7G(5′)ppp(5′)G RNA cap structure analog	New England Biolabs	Cat#: S1404S
G(5′)ppp(5′)A RNA Cap Structure Analog	New England Biolabs	Cat#: S1406S
AMP-PNP	Sigma-Aldrich	Cat#: 10102547001
Biotin-11-ATP	Perkin Elmer	Cat#: NEL544001EA
Biotin-11-UTP	Perkin Elmer	Cat#: NEL543001EA
His6-eIF4A1	This Paper	N/A
RNaseI	Ambion	Cat#: AM2294
M-MuLV	New England Biolabs	Cat#: M0253L
DMRIE-C	ThermoFisher	Cat#: 10459014
Turbo DNase	LifeTech	Cat#: AM2239
RNaseI	LifeTech	Cat#: AM2295
FastAP	LifeTech	Cat#: EF0652
Murine RNase Inhibitor	New England Biolabs	Cat#: M0314L
T4 PNK	New England Biolabs	Cat#: M0201L
T4 RNA ligase 1 high concentration	New England Biolabs	Cat#: M0437M
Proteinase K	New England Biolabs	Cat#: P8107S
Q5 PCR Master Mix	New England Biolabs	Cat#: M0494L
AffinityScript Reverse Transcriptase	Agilent	Cat#: 600107
Exo-SAP-IT	Affymetrix	Cat#: 78201
Critical Commercial Assays		
DC Protein Assay	Bio-Rad	Cat#: 5000112
Rabbit Reticulocyte Lysate	Promega	Cat#: L4960
5x Passive Lysis Buffer	Promega	Cat#: E1941

REAGENT or RESOURCE	SOURCE	IDENTIFIER
Anti-FLAG magnetic beads	Sigma	Cat#: M8823
Agencourt AMPure XP beads	Beckman Coulter	Cat#: A63881
Dynabeads MyOne Silane	LifeTech	Cat#: 37002D
Experimental Models: Cell Lines		
Mouse: NIH/3T3	ATCC	RRID: CVCL_0594
Mouse: eIF4A1^{em1JP}	NIH/3T3 cell line generated through CRISPR/Cas9 editing (Chu et al., 2016)	N/A
Human: HEK293T 3xFLAG-eIF4A1	This Paper	N/A
Oligonucleotides		
5′ 6-FAM (Fluorescein)	Integrated DNA Technologies	N/A
Random Hexamers	New England Biolabs	Cat#: S1330S
A full list of oligos	See Table S3	N/A
Recombinant DNA		
pET15b-His6-eIF4A	PMID: 16030146	N/A
pKS-FF-HCV-Ren	PMID: 14769948	N/A
LeGo-mU6-sg4A1-Cas9(D10A)	This Paper	N/A
Software and Algorithms		
Prism 7.0c	Graphpad	https://www.graphpad.com/
Bowtie	PMID: 19261174	Version 1.1.1
Cutadapt	https://cutadapt.readthedocs.io/en/stable/installation.html	Version 1.2.1
Python	https://www.python.org/downloads/release/python-276/	Version 2.7.6
Other		
RefSeq Transcriptome Catalogue	PMID: 26553804	Version 80
eCLIP Data	https://www.ncbi.nlm.nih.gov/geo/query/acc.cgi?acc=GSE142338	GSE142338